Progress In Electromagnetics Research Letters, Vol. 122, 67-74, 2024

PIER Letters

(Received 1 April 2024, Accepted 15 August 2024, Scheduled 27 August 2024)

Study on the Two-Load Transmission Characteristics of a WPT System with Double Transmitting Coils

Suqi Liu[1,*], Xueying Yan[1], and Yuping Liu[2]

[1]College of Mechanical and Electrical Engineering, Guilin University of Electronic Technology, Guilin 541004, China
[2]College of Electronic Engineering and Automation, Guilin University of Electronic Technology, Guilin 541004, China

ABSTRACT: It is expensive that each consuming power equipment needs to equip a separate wireless power charger. In addition, obtaining constant output power and high transfer efficiency in large coupling variation ranges is challenging. In this study, the two-load transmission characteristics of a WPT system with double transmitting coils are studied. The circuit model of the two-load WPT system is first developed, and the transmission characteristics are studied. The two-load WPT system achieving constant output power and transmission efficiency is then studied. Finally, the two-load WPT experimental system is designed. This system can achieve self-adjusting impedance compensation. Moreover, constant output power and transmission efficiency are achieved in each receiver, where their fluctuations are less than 5%. Furthermore, the utilization of the charger is improved by more than 8% due to the two receivers. This topology can provide a solution for practical application problems, such as the two-load wireless charger of the vehicle mobile phone.

1. INTRODUCTION

Wireless power transfer (WPT) [1, 2] has been widely adopted in industry, such as in electric vehicles, consumer electronics, and military [3, 4].

However, at present, the existing traditional WPT chargers can accept only a single load. In other words, their system cannot meet the demands of multiple devices. Therefore, a high demand on multi-load WPT systems has evolved [5].

In practical applications, the output power and transmission efficiency are unsteady and very sensitive to the coupling distance, because the system undergoes the frequency splitting phenomenon [6, 7]. This leads to the occurrence of the vibration phenomenon of the receiver-coil (or relay-coil) in a three-coil WPT system, because of the existence of frequency splitting [8, 9]. Thus, the WPT system is rather sensitive to the distance and alignment changes among the coils. Any change in the coil coupling distance and alignment from the initial optimal position and orientation results in degraded output power and transmission efficiency [6]. In other words, it is a challenge to obtain constant output power and transfer efficiency in large coupling variation ranges.

It is known that, if the WPT system obtains the optimal impedance, the maximum output power and transmission efficiency can be obtained [10]. It has been shown in [11] that the determination of the impedance zones on the two sides of the secondary compensation network based on various constraints, followed by selection of the compensation topology and parameters for performing the desired mapping between the impedance zones, allows the optimization of system performance. The authors of [12] proposed a novel parameter design method based on double-sided inductance-capacitance-capacitance (LCC) compensation topology, while considering the impact of the primary phase angle (PPA) and secondary phase angle (SPA) on the system efficiency. In the study presented in [13], the WPT system achieves the dynamic impedance compensation by adding or removing the inductances or capacitances from the compensator. However, it suffers from a transient shock. In the study presented in [14], a method is proposed to perform self-adjustment of the impedance compensator using two series transmitting coils. Consequently, due to the variations of the transmission distance and orientation of the coils, constant output power and transmission efficiency are obtained.

Based on the aforementioned results, a topology of the two-load WPT system with double transmitting coils is proposed. It can perform self-adjusting impedance compensation, and constant output power and transmission efficiency are achieved in each receiver in a fixed-frequency mode. The circuit model is first developed, and the transmission characteristics are analyzed. The output power and transmission efficiency are then simulated by adopting the Biot-Savart law and using the MATLAB software. Afterwards, a two-load WPT experimental system is developed. Constant output power and transmission efficiency are achieved in each receiver in a fixed-frequency mode, with fluctuations less than 5%. Furthermore, the utilization of the charger is improved by more than 8% due to the two receivers. This topology is able to provide a solution in practical applications, such as the two-load wireless charger of the vehicle mobile phone.

2. MODELING OF THE TWO-LOAD WPT SYSTEM

In the study presented in [14], the system obtains a uniform magnetic field by applying double transmitting coils. Constant

* Corresponding author: Suqi Liu (liusuqi2009@126.com).

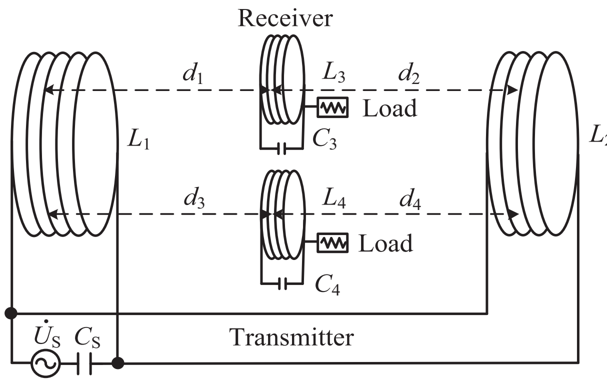

FIGURE 1. Sketch of the two-load WPT system with double transmitting coils (L_1 and L_2).

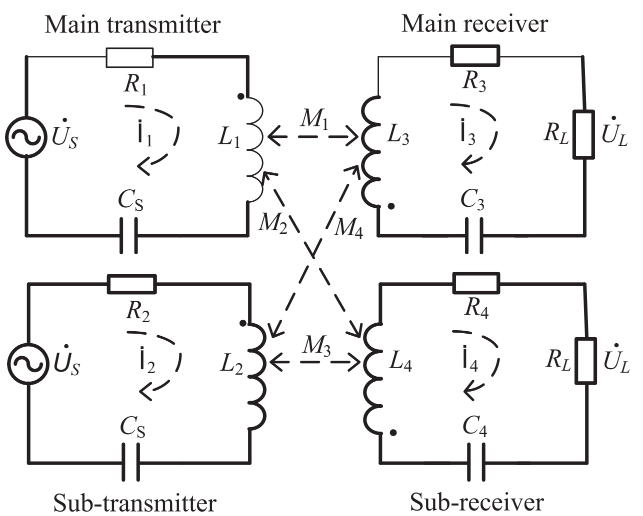

FIGURE 2. Equivalent circuit of the two-load WPT system with double transmitting coils.

output power and high transmission efficiency are also obtained in a fixed-frequency mode. Based on aforementioned results, this paper presents a topology of the two-load WPT system with double transmitting coils. The two-load transmission characteristics with double transmitting coils are then studied.

A diagram of the two-load WPT system with double transmitting coils is shown in Fig. 1, where constant output power and transmission efficiency with two loads are achieved. A sketch of the two-load WPT system with double transmitting coils (L_1 and L_2) is shown in Fig. 2. The double transmitting coils are linked into the transmitter loop, and the main transmitter (M-Tx) and sub-transmitter (S-Tx) loops are then created using the same circuit of the transmitter, as shown in Fig. 2.

The parameters of this two-load WPT system are shown in Table 1. Note that, for the convenience of analysis, the mutual inductance of the M-Tx and S-Tx coils is ignored because M_1, M_2, M_3, and M_4 are much larger. The mutual inductance of the M-Rx and S-Rx coils is also ignored.

A convenient reference for the analysis of the transmission characteristics of a two-load WPT system is provided by the equivalent circuit model. The assumed parameters of the M-Tx, S-Tx, M-Rx, and S-Rx are presented in Table 2.

TABLE 1. Parameters of the two-load WPT system.

Parameter	Value
Input power	$\dot{U}_S$
Load voltage	$\dot{U}_L$
Winding ohmic resistance of the coil	R_1, R_2, R_3, R_4
Load resistance	R_L
Inductance of the coil	L_1, L_2, L_3, L_4
Capacitance	C_S, C_3, C_4
Coupling distance	d_1, d_2, d_3, d_4, d_5 $= d_1 + d_2$or $d_5 = d_3 + d_4$
Mutual inductance	$M1, M_2, M_3, M_4$

The two-load WPT system with double transmitting coils can be written as:

$$\begin{cases} Z_1\dot{I}_1 - j\omega M_1\dot{I}_3 - j\omega M_2\dot{I}_4 = \dot{U}_S \\ Z_2\dot{I}_2 - j\omega M_3\dot{I}_4 - j\omega M_4\dot{I}_3 = \dot{U}_S \\ Z_3\dot{I}_3 - j\omega M_1\dot{I}_1 - j\omega M_4\dot{I}_2 = 0 \\ Z_4\dot{I}_4 - j\omega M_2\dot{I}_1 - j\omega M_3\dot{I}_2 = 0 \end{cases} \tag{1}$$

where ω is the driving source of angular frequency.

The self-impedances of M-Tx Z_1, S-Tx Z_2, M-Rx Z_3, and S-Rx Z_4 are given by [13]:

$$\begin{cases} Z_1 = Z_2 = R_1 + j\omega L_1 + \frac{1}{j\omega C_S} \\ \quad = (\sigma + \frac{j\omega_0 L}{R}\frac{\omega}{\omega_0} + \frac{1}{j\omega_0 CR}\frac{\omega_0}{\omega})R = (\sigma + j\xi)R \\ Z_3 = Z_4 = R_3 + R_L + j\omega L_3 + \frac{1}{j\omega C_3} \\ \quad = (1 + \frac{j\omega_0 L}{R}\frac{\omega}{\omega_0} + \frac{1}{j\omega_0 CR}\frac{\omega_0}{\omega})R = (1 + j\xi)R \end{cases} \tag{2}$$

The impedance coupling factors $\tau_1\tau_2$, τ_3, and τ_4, which indicate the ability of the impedance coupling [13], are given by:

$$\begin{cases} \tau_1 = \frac{\omega M_1}{\sqrt{R_1(R_3+R_L)}} = \frac{\omega M_1}{\sqrt{\sigma}R}, \quad \tau_1 > 0 \\ \tau_2 = \frac{\omega M_2}{\sqrt{R_1(R_4+R_L)}} = \frac{\omega M_2}{\sqrt{\sigma}R}, \quad \tau_2 > 0 \\ \tau_3 = \frac{\omega M_3}{\sqrt{R_2(R_4+R_L)}} = \frac{\omega M_3}{\sqrt{\sigma}R}, \quad \tau_3 > 0 \\ \tau_4 = \frac{\omega M_4}{\sqrt{R_2(R_3+R_L)}} = \frac{\omega M_4}{\sqrt{\sigma}R}, \quad \tau_4 > 0 \end{cases} \tag{3}$$

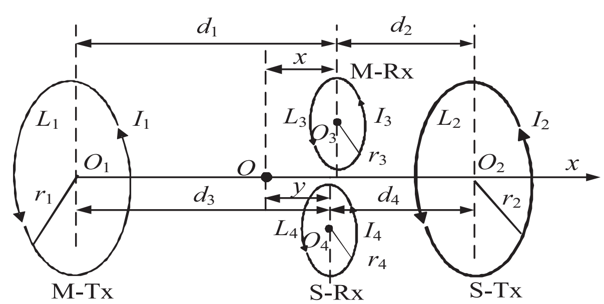

FIGURE 3. Sketch of the mutual inductance of the two-load WPT system, which includes the M-Tx coil L_1, S-Tx coil L_2, M-Rx coil L_3, and S-Rx coil L_4.

TABLE 2. Assumed values for the individual circuit elements of the M-T$_X$, S-T$_X$, M-R$_X$, and S-R$_X$.

Parameter	Value
Capacitances	$C_S = C_3 = C_4 = C$
Inductances	$L_1 = L_2 = L_3 = L_4 = L$
Resistance	$R_3 + R_L = R_4 + R_L = R$
Ratio	$R_L = \beta R\ (0 < \beta < 1)$, $R_1 = R_2 = \sigma R\ (\sigma > 0)$
Resonance frequency	$f = \omega/2\pi$
Frequency detuning factor	$\xi = Q(\omega/\omega - \omega/\omega)$
Resonant angular frequency	$\omega = 1/(LC)^{0.5}$, $\omega_1 = \omega_2 = \omega_3 = \omega_4 = \omega$
Quality factor	$Q = \omega L/R = 1/(\omega CR)$, $Q_1 = Q_2 = \omega L/R_1 = 1/(\omega CR_1) = Q/\sigma$, $Q_3 = Q_4 = \omega L/(R_4 + R_L) = 1/(\omega C(R_4 + R_L)) = Q$

According to Equations (1), (2), and (3), and parameters of Table 2, the currents can be expressed as:

$$\begin{cases} \dot{I}_1 = \dfrac{(1+j\xi)\left[(1+j\xi)(\sigma+j\xi)+\sigma\left(\tau_3^2+\tau_4^2-\tau_1\tau_4-\tau_2\tau_3\right)\right]}{(1+j\xi)^2(\sigma+j\xi)^2+\sigma(1+j\xi)(\sigma+j\xi)\left(\tau_1^2+\tau_2^2+\tau_3^2+\tau_3^4\right)+\sigma^2\left(\tau_1^2\tau_3^2+\tau_2^2\tau_4^2-2\tau_1\tau_3\tau_2\tau_4\right)}\dfrac{\dot{U}_S}{R} \\ \dot{I}_2 = \dfrac{(1+j\xi)\left[(1+j\xi)(\sigma+j\xi)+\sigma\left(\tau_1^2+\tau_2^2-\tau_1\tau_4-\tau_2\tau_3\right)\right]}{(1+j\xi)^2(\sigma+j\xi)^2+\sigma(1+j\xi)(\sigma+j\xi)\left(\tau_1^2+\tau_2^2+\tau_3^2+\tau_3^4\right)+\sigma^2\left(\tau_1^2\tau_3^2+\tau_2^2\tau_4^2-2\tau_1\tau_3\tau_2\tau_4\right)}\dfrac{\dot{U}_S}{R} \\ \dot{I}_3 = j\dfrac{\sqrt{\sigma}\left[(1+j\xi)(\sigma+j\xi)(\tau_1+\tau_4)+\sigma\left(\tau_1\tau_3^2+\tau_4\tau_2^2-\tau_1\tau_2\tau_4-\tau_2\tau_3\tau_4\right)\right]}{(1+j\xi)^2(\sigma+j\xi)^2+\sigma(1+j\xi)(\sigma+j\xi)\left(\tau_1^2+\tau_2^2+\tau_3^2+\tau_3^4\right)+\sigma^2\left(\tau_1^2\tau_3^2+\tau_2^2\tau_4^2-2\tau_1\tau_3\tau_2\tau_4\right)}\dfrac{\dot{U}_S}{R} \\ \dot{I}_4 = j\dfrac{\sqrt{\sigma}\left[(1+j\xi)(\sigma+j\xi)(\tau_1+\tau_4)+\sigma\left(\tau_3\tau_1^2+\tau_2\tau_4^2-\tau_1\tau_2\tau_4-\tau_1\tau_3\tau_4\right)\right]}{(1+j\xi)^2(\sigma+j\xi)^2+\sigma(1+j\xi)(\sigma+j\xi)\left(\tau_1^2+\tau_2^2+\tau_3^2+\tau_3^4\right)+\sigma^2\left(\tau_1^2\tau_3^2+\tau_2^2\tau_4^2-2\tau_1\tau_3\tau_2\tau_4\right)}\dfrac{\dot{U}_S}{R} \end{cases} \tag{4}$$

By applying Equation (4), the output powers of the M-Rx P_M and S-Rx P_S are respectively written in Equations (5) and (6), and the transmission efficiencies of the M-Rx η_M and S-Rx η_S are presented in Equations (7) and (8), respectively. By assuming that $\partial P_M/\partial\xi$ and $\partial P_S/\partial\xi$ are null, the WPT system has three roots [16]. By applying these roots, the system achieves a maximum output power (P_{outmax}) of $(\beta U_S^2)/(4\sigma R)$. Thus, the normalized output powers of M-Rx and S-Rx can be written as $\psi_M = P_M/P_{\text{outmax}}$ and $\psi_S = P_S/P_{\text{outmax}}$, respectively.

$$\begin{aligned} P_M =& |\dot{I}_3|^2 R_L \\ =& \Big\{\beta\sigma\Big\{\xi^2(1+\sigma)^2(\tau_1+\tau_4)^2+\left[(\tau_1+\tau_4)\left(\sigma-\xi^2\right)\right. \\ &\left.+\sigma\left(\tau_1\tau_3^2+\tau_2\tau_4^2-\tau_1\tau_2\tau_3-\tau_2\tau_3\tau_4\right)\right]^2\Big\}\dot{U}_S^2\Big\}\Big/ \\ & R\Big\{\xi^2\left[3\sigma(1+\sigma)+2\xi^2(1-\sigma)\right]^2 \\ &+\left[\xi^4-\xi^3-\left(\sigma^2+4\sigma\right)\xi^2+\sigma^2\right. \\ &+\sigma\left(\sigma-\xi^2\right)\left(\tau_1^2+\tau_2^2+\tau_3^2+\tau_4^2\right) \\ &\left.+\sigma^2\left(\tau_1^2\tau_3^2+\tau_2^2\tau_4^2-2\tau_1\tau_2\tau_3\tau_4\right)\right]^2\Big\} \end{aligned} \tag{5}$$

$$\begin{aligned} P_S =& |\dot{I}_4|^2 R_L \\ =& \Big\{\beta\sigma\Big\{\xi^2(1+\sigma)^2(\tau_1+\tau_4)^2+\left[(\tau_1+\tau_4)\left(\sigma-\xi^2\right)\right. \\ &\left.+\sigma\left(\tau_1^2\tau_3+\tau_2^2\tau_4-\tau_1\tau_2\tau_3-\tau_2\tau_3\tau_4\right)\right]^2\Big\}\dot{U}_S^2\Big\}\Big/ \\ & R\Big\{\xi^2\left[3\sigma(1+\sigma)+2\xi^2(1-\sigma)\right]^2 \\ &+\left[\xi^4-\xi^3-\left(\sigma^2+4\sigma\right)\xi^2+\sigma^2\right. \\ &+\sigma\left(\sigma-\xi^2\right)\left(\tau_1^2+\tau_2^2+\tau_3^2+\tau_4^2\right) \\ &\left.+\sigma^2\left(\tau_1^2\tau_3^2+\tau_2^2\tau_4^2-2\tau_1\tau_2\tau_3\tau_4\right)\right]^2\Big\} \end{aligned} \tag{6}$$

$$\begin{aligned} \eta_M =& \frac{P_M}{P_{in}} \\ =& \frac{|\dot{I}_3|^2 R_L}{|i_1|^2 R_1+|i_2|^2 R_2+|i_3|^2(R_3+R_L)+|i_4|^2(R_4+R_L)} \\ =& \beta\Big\{\xi^2(1+\sigma)^2(\tau_1+\tau_4)^2+\left[(\tau_1+\tau_4)\left(\sigma-\xi^2\right)\right. \\ &\left.+\sigma\left(\tau_1\tau_3^2+\tau_2\tau_4^2-\tau_1\tau_2\tau_3-\tau_2\tau_3\tau_4\right)\right]^2\Big\}\Big/ \\ & \Big\{\xi^2(1+\sigma)^2(\tau_1+\tau_4)^2+\left[\left(\sigma-\xi^2\right)(\tau_1+\tau_4)\right. \\ &\left.+\sigma\left(\tau_1\tau_3^2+\tau_2\tau_4^2-\tau_1\tau_2\tau_3-\tau_2\tau_3\tau_4\right)\right]^2 \\ &+\left(1+\xi^2\right)\Big\{2\xi^2(1+\sigma)^2-\left[\xi^2+\sigma\right. \\ &\left.+\sigma\left(\tau_3^2+\tau_4^2-\tau_1\tau_4-\tau_2\tau_3\right)\right]^2 \\ &-\left[\xi^2+\sigma+\sigma\left(\tau_1^2+\tau_2^2-\tau_1\tau_4-\tau_2\tau_3\right)\right]^2\Big\}\Big\} \end{aligned} \tag{7}$$

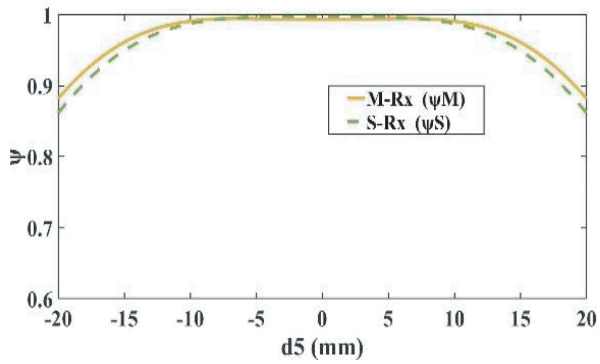

FIGURE 4. Characteristic curves of the normalized output powers of M-Rx ψ_M and S-Rx ψ_S using the electromagnetic field superposition principle, with $\xi = 0.265$ and $d_3 = 32$ mm.

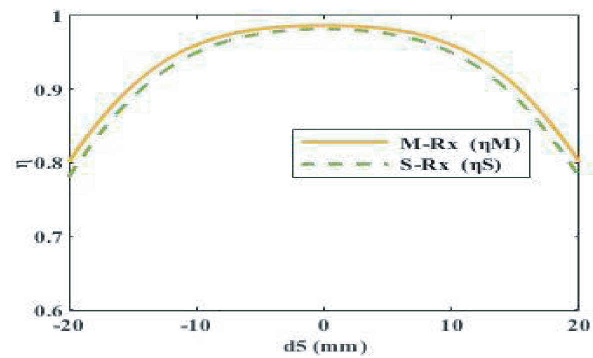

FIGURE 5. Characteristic curves of the normalized transmission efficiencies of M-Rx η_M and S-Rx η_S using the electromagnetic field superposition principle, with $\xi = 0.265$ and $d_3 = 32$ mm.

$$
\begin{aligned}
\eta_S &= \frac{P_S}{P_{in}} \\
&= \frac{|\dot{I}_4|^2 R_L}{|\dot{I}_1|^2 R_1 + |\dot{I}_2|^2 R_2 + |\dot{I}_3|^2 (R_3+R_L) + |\dot{I}_4|^2 (R_4+R_L)} \\
&= \beta\Big\{\xi^2(1+\sigma)^2(\tau_1+\tau_4)^2 + [(\tau_1+\tau_4)\left(\sigma-\xi^2\right) \\
&\quad + \sigma\left(\tau_1^2\tau_3 + \tau_2^2\tau_4 - \tau_1\tau_2\tau_3 - \tau_2\tau_3\tau_4\right)]^2\Big\} \Big/ \\
&\quad \Big\{\xi^2(1+\sigma)^2(\tau_1+\tau_4)^2 + \left[\left(\sigma-\xi^2\right)(\tau_1+\tau_4)\right. \\
&\quad \left. + \sigma\left(\tau_1\tau_3^2 + \tau_2\tau_4^2 - \tau_1\tau_2\tau_3 - \tau_2\tau_3\tau_4\right)\right]^2 \\
&\quad + \left(1+\xi^2\right)\Big\{2\xi^2(1+\sigma)^2 - \left[\xi^2 + \sigma\right. \\
&\quad \left. + \sigma\left(\tau_3^2 + \tau_4^2 - \tau_1\tau_4 - \tau_2\tau_3\right)\right]^2 \\
&\quad - \left[\xi^2 + \sigma + \sigma\left(\tau_1^2 + \tau_2^2 - \tau_1\tau_4 - \tau_2\tau_3\right)\right]^2\Big\}\Big\}
\end{aligned} \tag{8}
$$

3. ANALYSIS OF THE TWO-LOAD WPT SYSTEM

Figure 3 shows a sketch of the mutual inductance of the two-load WPT system that uses double transmitting coils. Note that each receiver achieves constant output power and transmission efficiency. The underlying parameters are determined by the Biot-Savart law and the mutual inductance shown in Fig. 3. They are presented in Table 3.

The M_1, M_2, M_3, and M_4 mutual inductances can be determined according to the magnetic induction intensities B_1, B_2, B_3, and B_4 [15], and the mutual inductance shown in Fig. 3:

$$
\begin{cases}
M_1 = \frac{\Phi_1}{\dot{I}_1} = \frac{\pi r_3^2 B_1}{\dot{I}_1} = \frac{\pi\mu_0 (n_1 n_3)^{0.5} (r_1 r_3)^2}{2(r_1^2+d_1^2)^{3/2}} \\
M_2 = \frac{\Phi_2}{\dot{I}_2} = \frac{\pi r_3^2 B_2}{\dot{I}_2} = \frac{\pi\mu_0 (n_2 n_3)^{0.5} (r_2 r_3)^2}{2(r_2^2+d_2^2)^{3/2}} \\
M_3 = \frac{\Phi_3}{\dot{I}_1} = \frac{\pi r_4^2 B_3}{\dot{I}_1} = \frac{\pi\mu_0 (n_1 n_4)^{0.5} (r_1 r_4)^2}{2(r_1^2+d_3^2)^{3/2}} \\
M_4 = \frac{\Phi_4}{\dot{I}_2} = \frac{\pi r_4^2 B_4}{\dot{I}_2} = \frac{\pi\mu_0 (n_2 n_4)^{0.5} (r_2 r_4)^2}{2(r_2^2+d_4^2)^{3/2}}
\end{cases} \tag{9}
$$

According to Equations (3) and (9), the τ_1, τ_2, τ_3, and τ_4 impedance coupling factors can be rewritten as:

$$
\begin{cases}
\tau_1 = \frac{\pi\omega\mu_0 (n_1 n_3)^{0.5} (r_1 r_3)^2}{2\sqrt{\sigma} R (r_1^2+d_1^2)^{3/2}} = \frac{\pi\omega\mu_0 (n_1 n_3)^{0.5} (r_1 r_3)^2}{2\sqrt{\sigma} R (r_1^2+(\frac{d_1+d_2}{2}+x)^2)^{3/2}} \\
\tau_2 = \frac{\pi\omega\mu_0 (n_2 n_3)^{0.5} (r_1 r_4)^2}{2\sqrt{\sigma} R (r_1^2+d_1^2)^{3/2}} = \frac{\pi\omega\mu_0 (n_1 n_4)^{0.5} (r_1 r_4)^2}{2\sqrt{\sigma} R (r_1^2+(\frac{d_1+d_2}{2}-x)^2)^{3/2}} \\
\tau_3 = \frac{\pi\omega\mu_0 (n_2 n_4)^{0.5} (r_2 r_4)^2}{2\sqrt{\sigma} R (r_2^2+d_2^2)^{3/2}} = \frac{\pi\omega\mu_0 (n_2 n_4)^{0.5} (r_2 r_4)^2}{2\sqrt{\sigma} R (r_2^2+(\frac{d_1+d_2}{2}+y)^2)^{3/2}} \\
\tau_4 = \frac{\pi\omega\mu_0 (n_2 n_3)^{0.5} (r_2 r_3)^2}{2\sqrt{\sigma} R (r_2^2+d_2^2)^{3/2}} = \frac{\pi\omega\mu_0 (n_2 n_3)^{0.5} (r_2 r_3)^2}{2\sqrt{\sigma} R (r_2^2+(\frac{d_1+d_2}{2}-y)^2)^{3/2}}
\end{cases} \tag{10}
$$

Based on Figs. 1–3, it is assumed that the coupling distances of the M-Tx and S-Tx coils ($d_5 = d_1 + d_2$ and $d_5 = d_3 + d_4$) have constant values of 32 mm and 40 mm, respectively. When the M-Rx coil (L_3) or S-Rx coil (L_4) moves from the M-Tx coil (L_1) to S-Tx coil (L_2), the coupling distance d_1 (or d_3) and $d_3 = d_5 - d_1$ (or d_4) are variable. The normalized output powers of M-Rx and S-Rx, determined based on Equations (5)–(8), are shown in Fig. 4. The transmission efficiencies of M-Rx and S-Rx are shown in Fig. 5. The normalized output powers of M-Rx and S-Rx, determined based on Equations (5)–(8), are illustrated in Fig. 6. The transmission efficiencies of M-Rx and S-Rx are presented in Fig. 7. This paper studies the two-load transmission characteristics of a WPT system with double transmitting coils.

It can be seen from Figs. 3–5 that, since the M-Tx and S-Tx coils are parallel, the output powers of O_3 and O_4 are obtained. Between points O_1 and O_2, the WPT system reaches constant output power and transmission efficiency of the M-Rx or S-Rx, because the double transmitting coils can determine the uniform magnetic field [16]. Outside points O_1 and O_2, the output power and transmission efficiency are significantly reduced.

Figure 6 shows the normalized output powers of M-Rx and S-Rx related to parameters σ, ξ, τ_1, τ_2, τ_3, and τ_4. Three states exist: (a) over-coupled region ($\tau_1 > 1$), (b) critical-coupled point ($\tau_1 = 1$), and (c) under-coupled region ($\tau_1 < 1$). In the over-coupled region, frequency splitting occurs, and thus the normalized output power reaches its maximum value. The maximum value of the normalized output power is obtained at the critical-coupled point. At the under-coupled region, the normalized output power significantly decreases. Based on the

TABLE 3. Parameters of the two-load WPT system of the magnetic induction intensity and geometric structure.

Parameter	Value
Magnetic induction intensity of the circular coil L_1 at the position of the coil L_3	$B_1 = \mu(n_1 n_3)^{0.5} r_1^2 I_1/(2(r_1^2 + d_1^2)^{3/2})$
Magnetic induction intensity of the circular coil L_2 at the position of the coil L_3	$B_2 = \mu(n_2 n_3)^{0.5} r_2^2 I_2/(2(r_2^2 + d_2^2)^{3/2})$
Magnetic induction intensity of the circular coil L_1 at the position of the coil L_4	$B_3 = \mu(n_1 n_4)^{0.5} r_1^2 I_1/(2(r_1^2 + d_3^2)^{3/2})$
Magnetic induction intensity of the circular coil L_2 at the position of the coil L_4	$B_4 = \mu(n_2 n_4)^{0.5} r_2^2 I_2/(2(r_2^2 + d_4^2)^{3/2})$
Radius of the M-Tx, S-Tx, M-Rx, and S-Rx coils	r_1, r_2, r_3, r_4
Permeability of vacuum (H/m)	$\mu = 4\pi \times 10^{-7}$
Turn number of the M-Tx, S-Tx, M-Rx, and S-Rx coils	n_1, n_2, n_3, n_4
Central point between the M-Tx and S-Tx coils	O
Geometric center of the M-Tx, S-Tx, M-Rx, and S-Rx coils	$O_1, O_2, O_3 O_4$
Magnetic flux of the magnetic field excited by the coil L_1 through the coil L_3	Φ_1
Magnetic flux of the magnetic field excited by the coil L_2 through the coil L_3	Φ_2
Magnetic flux of the magnetic field excited by the coil L_1 through the coil L_4	Φ_3
Magnetic flux of the magnetic field excited by the coil L_2 through the coil L_4	Φ_4

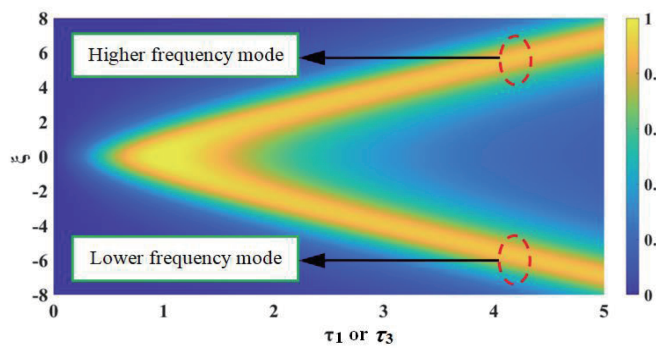

FIGURE 6. Characteristic curves of the output powers of M-Rx and S-Rx, for $\sigma = 2$, $\tau_2 = 0$, and $\tau_4 = 0$.

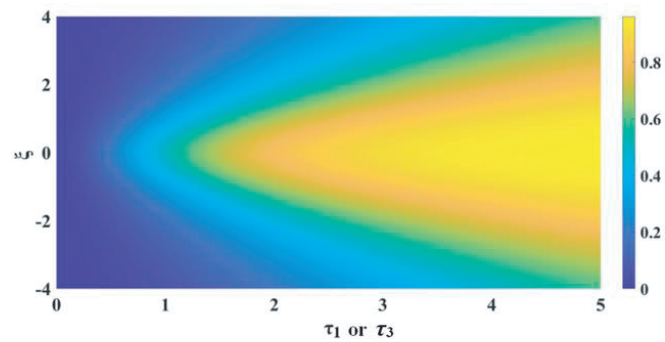

FIGURE 7. Characteristic curves of the transmission efficiencies of M-Rx and S-Rx, for $\beta = 1$, $\tau_2 = 0$, and $\tau_4 = 0$.

frequency detuning factor $\xi = Q(\omega/\omega 0 - \omega/\omega)$, the two-load WPT system achieves the maximum output power at the splitting angular frequencies ω_1 and ω_2, which belong to lower and higher frequency modes, respectively.

It can be observed from Fig. 7 that the transmission efficiency reaches its the maximum value at the resonance angular frequency ω. When τ_1 and τ_3 increase, the transmission efficiencies of the M-Rx and S-Rx gradually increase, respectively.

In summary, because the double transmitting coils of the two-load system can provide a uniform magnetic field, constant output power and transmission efficiency of M-Rx and S-Rx are obtained with a suitable transmitting distance d_5. In the sequel, experiments are first conducted, then the simulated and experimental results are compared.

4. EXPERIMENTAL RESULTS

The two-load WPT experimental block diagram is shown in Fig. 8 where D_1–D_4 are the rectifier diodes; C_K is the filter capacitor; and U_K is the DC voltage. The parameters of the two-load WPT experimental system are shown in Table 4.

The two-load experimental equipment includes the power amplifier, wave generator, voltage probes, capacitances, oscilloscope, transmitter, main receiver, sub-receiver, load, M-Tx coil, S-Tx coil, M-Rx coil, and S-Rx coil, as shown in Fig. 9.

The wave generator of the two-load WPT experimental system generates a sine signal, as shown in Figs. 8 and 9. The latter is amplified by the power amplifier. Sine power current flowed resonant circuit and power magnetic field are then generated. The M-Rx and S-Rx coils are put into the power magnetic field, and a high-frequency power current is induced. Afterwards, the power current is rectified and consumed by the two-load system.

In the experiments, d_5 is set to 20, 30, and 40 mm while d_1 or d_3 are set to 10, 15, and 20 mm. The input and output voltages and currents are measured at different frequencies. The results shown in Figs. 10–13 are obtained using these data. It can be seen from Figs. 10 and 11 that, when the transmission distances of the M-Tx and S-Tx coils are adjusted to 20 mm, the output power peaks of M-Rx and S-Rx occur at 125 kHz and 165 kHz, respectively. When d_5 is adjusted to 30 mm, the output power

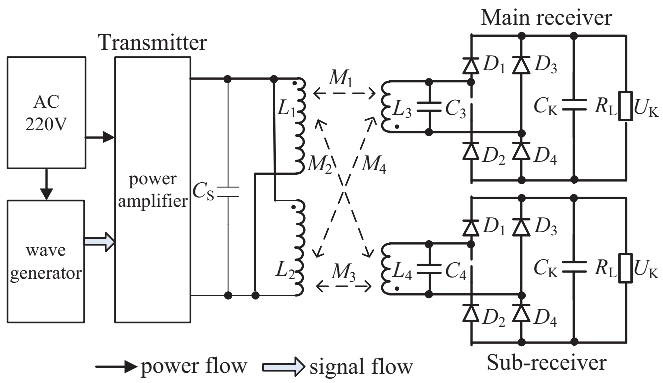

FIGURE 8. Experimental block diagram of the two-load WPT system that uses double transmitting coils to achieve constant output power and transmission efficiency.

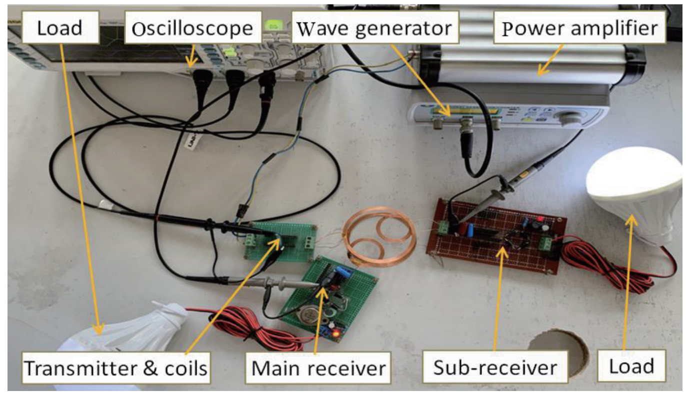

FIGURE 9. The two-load WPT experimental system that uses double transmitting coils to achieve constant output power and transmission efficiency.

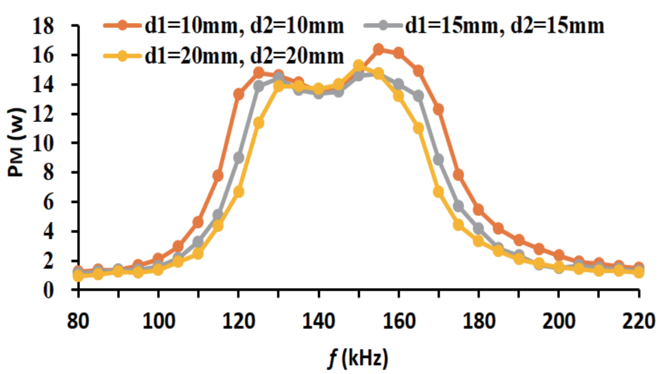

FIGURE 10. Output power of M-Rx function of the frequency.

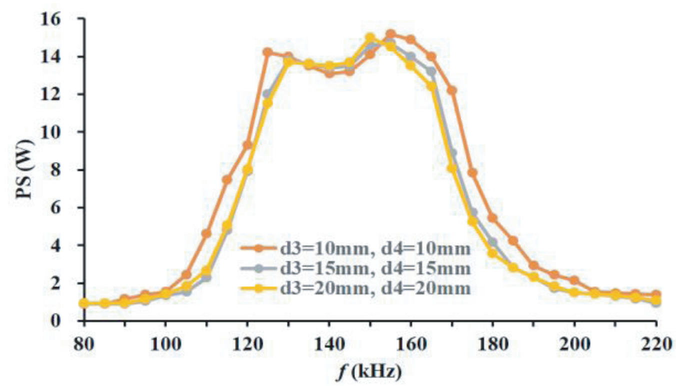

FIGURE 11. Output power of S-Rx function of the frequency.

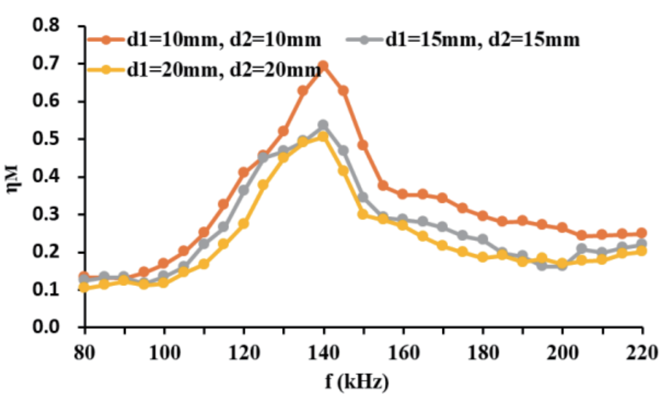

FIGURE 12. Transmission efficiency of M-Rx function of the frequency.

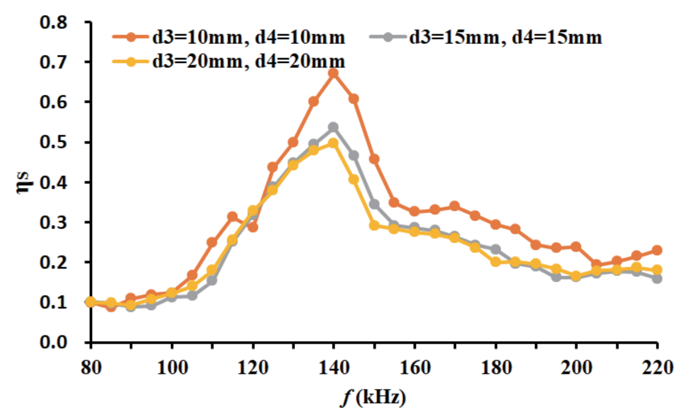

FIGURE 13. Transmission efficiency of S-Rx function of the frequency.

peaks of M-Rx and S-Rx occur at 130 kHz and 155 kHz, respectively. When $d5$ is adjusted to 40 mm, the output power peaks of M-Rx and S-Rx occur at 150 kHz. It can be seen from Figs. 12 and 13 that, when d_5 is adjusted to 20, 30, and 40 mm, M-Rx and S-Rx attain their maximum transmission efficiencies at 150 kHz. When d_5 decreases, the transmission efficiency increases and its curves move to the higher frequency direction.

It can then be deduced that, when $d_5 = 20$ mm, the output powers of M-Rx and S-Rx reach their maximum values at 125 kHz and 165 kHz, respectively. When $d_5 = 30$ mm, the output powers of M-Rx and S-Rx reach their maximum values at 130 kHz and 155 kHz, respectively. When $d_5 = 40$ mm, the output powers of M-Rx and S-Rx reach their maximum values at 150 kHz. If the driving source of frequency is increased, the aforementioned frequencies remain constant when the two-

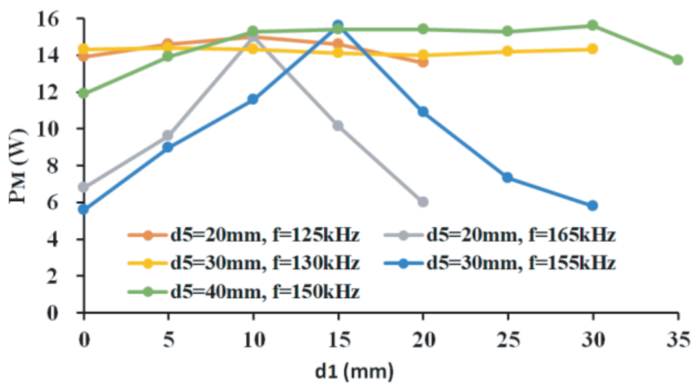

FIGURE 14. Output power of M-Rx function of the distance.

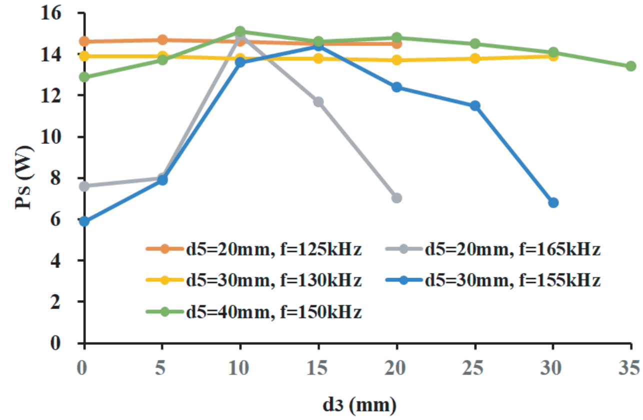

FIGURE 15. Output power of S-Rx function of the distance.

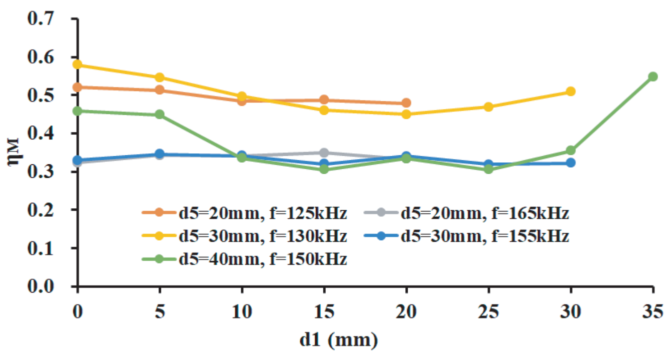

FIGURE 16. Transmission efficiency of M-Rx function of the distance.

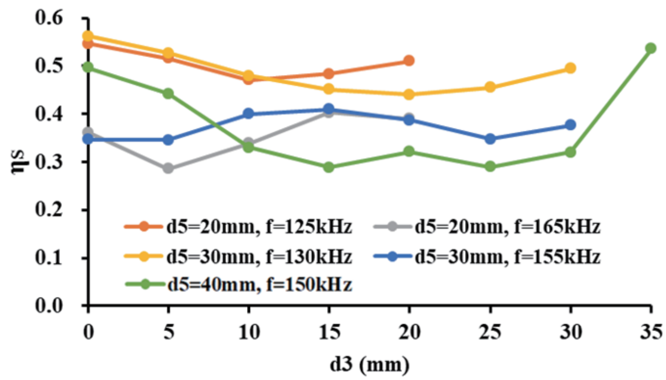

FIGURE 17. Transmission efficiency of S-Rx function of the distance.

TABLE 4. Parameters of the transmitter (M-Tx and S-Tx), main receiver (M-Tx), and sub-receiver (M-Rx) of the MCR-WPT system.

Parameter	M_Tx or S_Tx	M-Rx or S-Rx
Inside diameter of the coil φ/m	$68 * 10^{-3}$	$30 * 10^{-3}$
Outside diameter of the coil Φ/m	$78 * 10^{-3}$	$38 * 10^{-3}$
Layers of the coil	3	3
Number of turns n	20	20
Frequency f/kHz	140	140
Inductance L/μH	58.5	29.25
Capacitance C/nF	11.45	22.09
Distance $d_5 = d_1 + d_2$ mm	20, 30, or 40	
Impedance scaling factor σ	2	
Frequency detuning factor ξ	0.265	
Load R_L Ω	0.5	
Input Voltage V	20	
Input power W	40	

load system functions. When d_5 is constant, the input and output voltages are measured in the case where d_1 or d_3 changes (i.e., the M-Rx or S-Rx coils moves from the M-Tx coil to the STx coils). The input and output currents of the system are also measured. The obtained results are shown in Figs. 14–17. It can be seen that, in the lower frequency mode (i.e., $d_5 = 20$ mm, $f = 125$ kHz; $d_5 = 30$ mm, $f = 130$ kHz; $d_5 = 40$ mm, $f = 155$ kHz), the output power and transmission efficiency reach constant values when d_1 or d_3 increases, with fluctuations less than 5%. However, in the higher frequency mode (i.e., $d_5 = 20$ mm, $f = 165$ kHz; $d_5 = 30$ mm, $f = 155$ kHz), when d_1 or d_3 increases, the transmission efficiency reaches its minimum value at point O, and the output power significantly decreases. In addition to the higher frequency mode, the experimental results are consistent with the simulated ones [14, 16].

Table 5 shows the output powers and transmission efficiencies of M-Rx and S-Rx for different distances. It can be seen that, for different distances, the fluctuations of the transmission efficiency and output power are less than 5% in each receiver.

TABLE 5. Output powers and transmission efficiencies of M-Rx and S-Rx for different distances.

d5/mm	P_M/W	P_S/W	η_M	η_S
20	14.51	14.56	0.491	0.492
30	14.42	14.12	0.492	0.488
40	14.45	14.42	0.396	0.368

In addition, in contrast to the results obtained in [14] and [16], the utilization of the charger is improved by more than 8% due to the existence of at least two receivers.

In general, the WPT system with double transmitting coils is a self-adjusting impedance compensator. More precisely, when it uses double transmitting coils and the coupling distance changes, it can perform impedance self-compensation. Therefore, the WPT system can always lead to constant output power and transmission efficiency.

5. DISCUSSION

In the considered topology, two receivers (or more) are placed between double transmitting coils. In fact, space limitations exist. Fig. 18 shows a feasible solution, where two mobile phones are simultaneously placed on the charging groove. Furthermore, by applying the proposed two-load WPT system, a new topology, incorporating small output power and transmission efficiency fluctuations in open space, can be established.

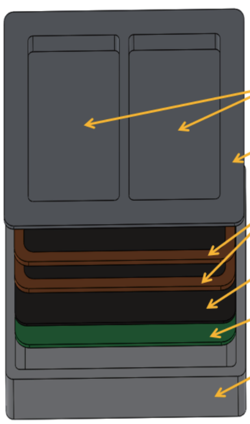

FIGURE 18. Explosion diagram of the two-load wireless charger for mobile phones.

6. CONCLUSION

This study proposes an efficient topology for a two-load WPT system which includes double transmitting coils. The transmission characteristics of the WPT system are simulated and analyzed by adopting the Biot-Savart law and using the MATLAB software. The main contributions and results can be summarized as follows:

(1) The developed WPT system with double transmitting coils is a self-adjusting impedance compensator. As long as the receiving coil moves between the two transmitting coils, constant output power and transmission efficiency can be obtained.

(2) In a fixed-frequency mode and lower frequency mode, the output power and transmission efficiency fluctuations of each receiver are less than 5%. More precisely, they obtain almost constant values in each receiver. In addition, the utilization of the charger is improved by more than 8% due to the existence of at least two receivers.

(3) This topology can provide an efficient solution for practical application issues, such as the two-load wireless charger of a vehicle mobile phone.

ACKNOWLEDGEMENT

This work was supported by the Guangxi Natural Science Foundation (2021JJA160252, 2021JJB160015); High Level Talent Foundation Project of Guilin University of Electronic Technology (UF20008Y).

REFERENCES

[1] Tesla, N., "Electrical energy," U.S. Patent, 1,119,732, 1914.

[2] Kurs, A., A. Karalis, R. Moffatt, J. D. Joannopoulos, P. Fisher, and M. Soljacic, "Wireless power transfer via strongly coupled magnetic resonances," *Science*, Vol. 317, No. 5834, 83–86, 2007.

[3] Chen, W., J. Liu, S. Chen, and L. Zhang, "Energy shaping control for wireless power transfer system in automatic guided vehicles," *Energies*, Vol. 13, No. 11, 2959, 2020.

[4] Khan, S. R., S. K. Pavuluri, G. Cummins, and M. P. Y. Desmulliez, "Miniaturized 3-D cross-type receiver for wirelessly powered capsule endoscopy," *IEEE Transactions on Microwave Theory and Techniques*, Vol. 67, No. 5, 1985–1993, 2019.

[5] Luo, C., D. Qiu, M. Lin, and B. Zhang, "Circuit model and analysis of multi-load wireless power transfer system based on parity-time symmetry," *Energies*, Vol. 13, No. 12, 3260, 2020.

[6] Gao, P., Z. Tian, T. Pan, J. Wu, and W. Gui, "Transmission efficiency analysis and optimization of magnetically coupled resonant wireless power transfer system with misalignments," *AIP Advances*, Vol. 8, No. 8, 085016, 2018.

[7] Sample, A. P., D. T. Meyer, and J. R. Smith, "Analysis, experimental results, and range adaptation of magnetically coupled resonators for wireless power transfer," *IEEE Transactions on Industrial Electronics*, Vol. 58, No. 2, 544–554, 2011.

[8] Liu, S., J. Tan, and X. Wen, "Modeling of coupling mechanism of wireless power transfer system and vibration phenomenon of receiver-coil in three-coil system," *AIP Advances*, Vol. 7, No. 11, 115107, 2017.

[9] Liu, S. and J. Tan, "Study on the vibration mechanism of the relay coil in a three-coil WPT system," *Progress In Electromagnetics Research M*, Vol. 70, 117–126, 2018.

[10] Xiao, C., Y. Liu, D. Cheng, and K. Wei, "New insight of maximum transferred power by matching capacitance of a wireless power transfer system," *Energies*, Vol. 10, No. 5, 688, 2017.

[11] Lu, S., M. Böttigheimer, and N. Parspour, "An impedance mapping-based t-compensation network and control strategy for WPT system with full-bridge active rectifier," *IEEE Transactions on Power Electronics*, Vol. 38, No. 11, 14 675–14 688, 2023.

[12] Sun, Z., J. Sun, Y. Wang, and D. Xu, "An efficiency optimization method based on double side impedance angle design for wireless power transfer system," *IEEE Transactions on Power Electronics*, Vol. 38, No. 4, 5000–5012, 2023.

[13] Liu, S. and J. Tan, "Dynamic impedance compensation for WPT using a compensator in a three-coil wireless power transfer system," *Circuit World*, Vol. 44, No. 4, 171–177, 2018.

[14] Liu, S. and Y. Liu, "Transfer characteristics of the MCR-WPT system using two series transmitting coils," *Circuit World*, Vol. 46, No. 1, 48–54, 2019.

[15] Xue, T., X. Meng, and L. Hou, "A new magnetic coupling mechanism for patrol robot wireless charging system," in *Journal of Physics: Conference Series*, Vol. 1639, No. 1, 012067, 2020.

[16] Liu, S. and J. Tan, "Using uniform magnetic field to obtain the constant output power and transfer efficiency for mcr-wpt," *Circuit World*, Vol. 46, No. 1, 42–47, 2019.